



Biosynthesis of ZnO/SiO₂ nanocatalyst with palash leaves' powder for treatment of petroleum refinery effluent



Rajani Bharati, S. Suresh*

Green Catalysis and Process Technology Research Laboratory, Department of Chemical Engineering, Maulana Azad National Institute of Technology, Bhopal 462 003, India

ARTICLE INFO

Article history:

Received 5 March 2017

Revised 30 June 2017

Accepted 15 August 2017

Available online 30 August 2017

Keywords:

ZnO/SiO₂ nanocatalyst

Green synthesis

Palash leaves

Treatment

Petroleum refinery

Effluent

ABSTRACT

This work aims the synthesis and characterization of ZnO/SiO₂ nanocatalyst from plant waste material by green route and application of this ZnO/SiO₂ nanocatalyst for the treatment of petroleum refinery effluent. *Butea monosperma* (Palash) leaves' powder was used as reducing and stabilizing agent for synthesis of ZnO/SiO₂ nanocatalyst. Palash leaves contain broad variability of biomolecules which work as reducing and capping agent. In this research work, COD and acenaphthylene which is Polycyclic Aromatic Hydrocarbons (PAH) were degraded by synthesizing ZnO/SiO₂ nanocatalyst under UV-light in an annular photocatalytic reactor. X-ray diffraction (XRD), Fourier transform infrared spectroscopy (FT-IR), FIELD emission gun-Scanning electron microscopy (FEG-SEM), Energy dispersive X-ray (EDX) and Transmission electron microscopy (TEM) analysis confirmed the formation of ZnO/SiO₂ nanocatalyst. Characterization studies revealed that spherical and hexagonal nanoparticles with particle size ranging from 8 ± 5 nm to 40 ± 5 nm and mean particle with diameter of 20 ± 5 nm were synthesized using this method which is stable in the environment. Brunauer, Emmett and Teller (BET) surface area of ZnO/SiO₂ nanocatalyst is found to be 150.25 m²/g. Fractional Factorial design was applied to find optimum condition of process parameters and found that optimum percent. Removal of COD (mg/l), and acenaphthylene were achieved at reaction condition of 1 g/L of ZnO/SiO₂ nanocatalyst loading, 30 °C temperature and 4 h reaction time and found that optimum percent removal of COD (mg/l), and acenaphthylene is 75%, and 73% respectively. Various metals, naturally present in palash leaves' powder, decrease band gap of energy and improve photocatalytic activity of nanocatalyst.

© 2017 Tomsk Polytechnic University. Published by Elsevier B.V.

This is an open access article under the CC BY-NC-ND license.

(<http://creativecommons.org/licenses/by-nc-nd/4.0/>)

1. Introduction

Petroleum refinery industries discharge highly polluted water, which creates health problems for human beings, disturbs ecosystem and also pollutes ground water so treatment of petroleum refinery effluent is a very big challenge before discharging of the contaminated water into the water bodies or environment. Petroleum refinery effluent contains Chemical Oxygen Demand (COD), Biological oxygen demand (BOD), total petroleum hydrocarbon (TPH), oil and grease (O & G), Sulphate and phenols as pollutants [1,2]. Petroleum refinery effluent contains many polycyclic aromatic hydrocarbons such as naphthalene, anthracene, acenaphthylene, acenaphthene, fluorene, phenanthrene etc. Photocatalytic degradation is a very effective treatment method which reduces an efficiently COD and hydrocarbons from wastewater [3,4]. The

characteristics of some petroleum refineries wastewater are given in Table 1.

The conventional treatment of refinery wastewater depends on the physicochemical and mechanical techniques and further biological treatments in the integrated activated sludge treatment units. Concerning the way that distinctive concentrations of aliphatic and aromatic petroleum hydrocarbons are available in refinery wastewaters, among which the aromatic fraction is not readily degraded by the conventional treatments and is more toxic, there is still a requirement for cutting edge strategies to reduce this kind of pollutants however much as could reasonably be expected. The photocatalysis is one of the procedures which can totally degrade the organic contaminations into safe inorganic substances, for example, CO₂ and H₂O under mild conditions.

Palash leaves have been using for biomedical purposes but it was not used for synthesis of nanocatalyst yet. Palash leaves contain many biomolecules these are Alkaloids, Phenolic acid, Flavonoids Carbohydrate and Protein which make it strong

* Corresponding author.

E-mail address: sureshpecchem@gmail.com (S. Suresh).

Table 1

Typical composition of some petroleum refinery effluents [23]. (Composition (mg/L).

| Parameters | Refinery –1 | Refinery –2 | Refinery-3 | Refinery- 4 |
|------------------|-------------|-------------|------------|-------------|
| pH | 7–9 | 6.5–7.5 | 8.0 | 10 |
| COD | 300–600 | 170–180 | 80–120 | 80.8 |
| BOD | 150–360 | – | 40.25 | 8.0 |
| PAH | 50–100 | 20–60 | 20–30 | 10–20 |
| O&G | <50 | NR | – | 45 |
| SS | <150 | 420–650 | 22.8 | NR |
| Ammonia | 15 | – | – | 22 |
| Phenols | – | – | – | 30 |
| Sulphides | 22 | 887 | – | 10 |

Table 2.

Characteristics of petroleum refinery wastewater Composition (mg/L).

| pH | COD | BOD | SS | PAH | Phenol | Sulphide | Oil-grease |
|------|-----|-----|-----|--------|--------|----------|------------|
| 8.76 | 550 | 250 | 110 | 50–100 | 90 | 5 | 500 |

Table 3.

The operative conditions of experiments.

| Parameter | Value |
|--|------------------------------|
| COD Concentration in refinery wastewater | Up to 550 mg/L ⁻¹ |
| Acenaphthylene in synthesis aqueous solution | Up to 100 mg/L ⁻¹ |
| pH | 3–11 |
| Temperature | 25–45 °C |
| Irradiation time | Up to 6 h |
| Light intensity | 11 W/m ² |
| Catalyst dose | 0.5 to 1.5 g/L |

Fractional Factorial Design

Factors: 5 Base Designs: 5, 8 Resolution: III

Runs: 24 Replicates: 3 Fraction: 1/4

Blocks: 1 Center pts (total): 0

biomass for synthesis of nanocatalyst. Functional groups present in flavonoids, carbohydrate, proteins work as reducing and stabilizing agent in chemical method coating surfactance are used for coating of functional group as stabilizing agent but in this method functional groups coated naturally. So in this experiments palash leaves powder has been used as reducing and stabilizing agent [5–9].

The object of the current research work is the green synthesis of enhanced photocatalyst of ZnO/SiO₂ nanocatalyst by using palash leaves' powder as reducing and stabilizing agent. After synthesis of nanocatalyst, various characterizations like XRD, FEG-SEM, TEM, FTIR, EDX, and BET were also carried out to know the size, morphology, and functional groups present in the nanocatalyst. To treat petroleum refinery effluent and increase the efficiency of nanocatalyst to reduce the concentration of acenaphthylene as PAH, and COD as pollutants from the petroleum refinery effluent. Palash leaves contain a wide range of biomolecules which work as reducing and stabilizing agent and thus increase the reaction rate of the synthesis of nanocatalyst. Palash leaves contain Protein, Carbohydrate etc. as biomolecules. Palash leaves also contain Si, Mg, S, K, Ca, and Cu, Zn metallic and nonmetallic elements naturally and thus increase photocatalytic activity of nanocatalyst [6]. The objec-

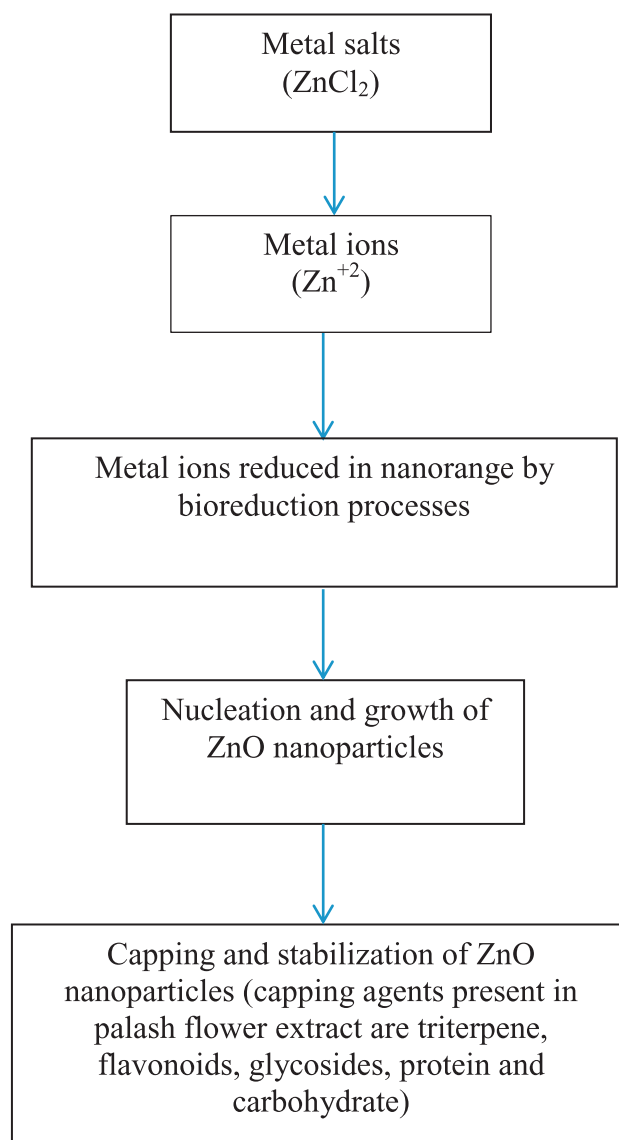


Fig. 1. Mechanism and role biomolecules present in palash leaves powder for nanocatalyst synthesis.

tive of this study is to optimize the operating parameters in photocatalytic degradation of COD and acenaphthylene using an annular reactor. ZnO/SiO₂ nanocatalyst was used in this study for refinery wastewater treatment. The operating parameters which include initial pollutant concentration, catalyst loading, initial wastewater pH, UV light intensity and operating temperature. Optimum parameter values depends on the target pollutant, type of catalyst and design of reactor used; hence there is a need to evaluate optimum operating parameter values for every new photocatalytic pol-

Table 4.

Factors and their levels used for two-levels used for two-level fractional factorial design for acenaphthylene.

| Factor name | Factor Code | Low level (–1) | High level (+1) |
|------------------------------------|-------------|----------------|-----------------|
| pH | A | 9.0 | 11.0 |
| Time (h) | B | 4 | 6 |
| Catalyst loading (g/L) | C | 1.0 | 1.5 |
| Initial concentration (mg/L) | D | 50 | 100 |
| Temperature (°C) | E | 25 | 30 |
| UV- Intensity (W/cm ²) | Constant | 11 | 11 |

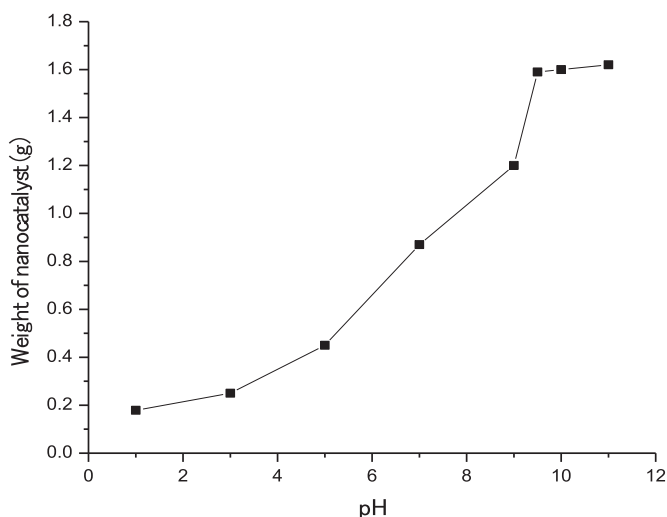


Fig. 2. Effect of pH on the yield of nanocatalyst by biosynthesis method for 1 liter of ZnO/SiO₂ solution.

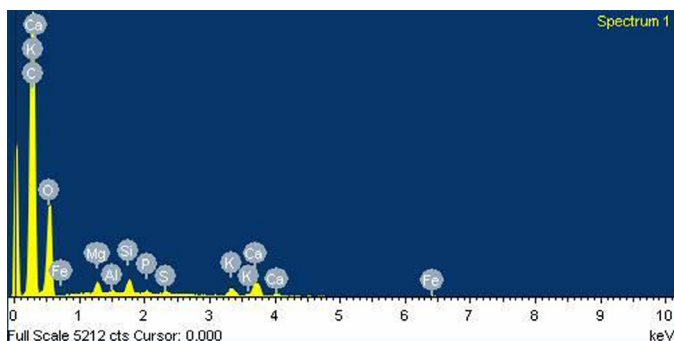


Fig. 3. EDX spectra of palash leaves powder before ZnO/SiO₂ nanocatalyst.

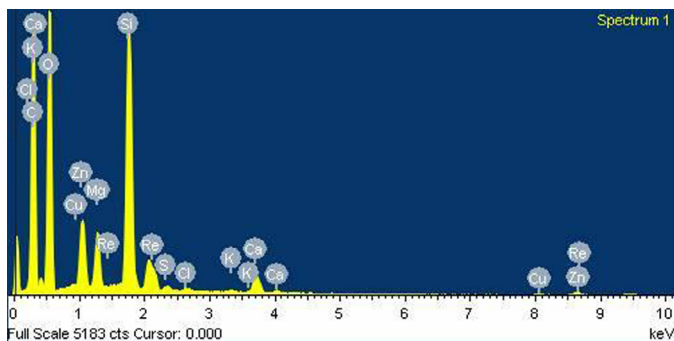


Fig. 4. EDX spectra for ZnO/SiO₂ nanocatalyst by Palash leaves powder.

lutant. In the present study, Fractional Factorial design was used in determining the optimum values of operating parameters in photocatalytic COD, acenaphthylene degradation using a photocatalytic reactor [10,11].

2. Materials and methods

2.1. Materials

Palash leaves were collected from MANIT campus Bhopal. ZnO (with 99% purity) was supplied by Molychem Company, Mumbai, HCl (36% purity) acid was used to make 1 M solution to dissolve ZnO in water; this Chemical was supplied by A. B. Enterprises, Mumbai. NaOH, to make a 1 N solution to change pH; was sup-

plied by A. B. Enterprises, Mumbai, and double distilled water; petroleum refinery effluent was collected from Northern petroleum refinery industry.

2.2. Methods

2.2.1. Synthesis of ZnO/SiO₂ nanocatalyst

For the synthesis of ZnO/SiO₂ nanocatalyst, by utilizing palash leaves' Powder as reducing and stabilizing agent, firstly the gathered palash leaves were washed and dried. Also, the dried palash leaves were processed and screened utilizing a 34 work strainer. For the synthesis of ZnO/SiO₂ nanocatalyst, a 0.5 g of dried Palash leaves' powder was added to 50 mL of 1 mM aqueous ZnO solution and heated at 60 °C for an h. It was found that ZnO is insoluble in water however in the wake of including a couple drops of 1 N HCl, it gets to be water dissolvable. The nanocatalyst of ZnO/SiO₂ accelerated at the base of the conical flask in the wake of taking 1 h as reaction time. A change in color of the solution from brownish yellow to dark brownish occurred, confirming the green synthesis of ZnO/SiO₂. The test was performed at various pH levels to know the impact of pH on nanocatalyst yield. The test was performed at pH level that range from 3 to 11. After the precipitation, the suspension over the precipitate was centrifuged at 10,000 rpm to isolate ZnO/SiO₂ nanocatalyst from biomass buildup. After partition, ZnO/SiO₂ nanocatalyst was dried at 60 °C in the oven.

2.3. Characterization

The characterization of ZnO/SiO₂ nanocatalyst was carried out by BET, EDX, FTIR, FEG-SEM, and XRD analysis. EDX, FEG-SEM, and TEM analyses were carried out at SAIF,

IIT Mumbai. FTIR and XRD analyses were carried out at central laboratory facility of North Maharashtra University, Jalgaon. BET analysis was carried out at Delhi University, Delhi to find the surface area of nanocatalyst. EDX analysis was carried out for elemental analysis of nanocatalyst, FTIR analysis was carried out to find functional groups present in ZnO/SiO₂ nanocatalyst, XRD analysis was carried out to find crystal structure of nanocatalyst and for phase identification. FEG-SEM analysis was carried out to find particle size, shape, and distribution of nanocatalyst.

2.4. Analytical method

Petroleum refinery wastewater for treatment was collected from Northern petroleum refinery. The composition of refinery wastewater was analyzed by standard EPA methods and has been shown in Table 2.

2.5. Treatment of petroleum refinery effluent with ZnO/SiO₂ nanocatalyst

Synthesized nanocatalyst was used to treat petroleum refinery effluent. Different catalyst loads were used to obtain optimum percent removal of pollutants. The catalyst concentration was varied as 0.5 g/L, 1.0 g/L and 1.5 g/L to treat petroleum refinery effluent. Various reaction parameters were set during the treatment of petroleum refinery effluent to find out their effect on the performance of photocatalytic reaction. These parameters were pH, reaction time, and catalyst loads, temperature and initial concentration. The pH range for treatment of petroleum refinery effluent was varied from 3 to 11 for COD removal. The pH was varied from 9 to 11 to find the effect of pH on percent removal of acenaphthylene, it is soluble in aqueous water sample at alkaline medium. The photocatalytic reaction, to treat petroleum refinery effluent in presence of UV-light, was performed for 6 h duration. To find the effect of

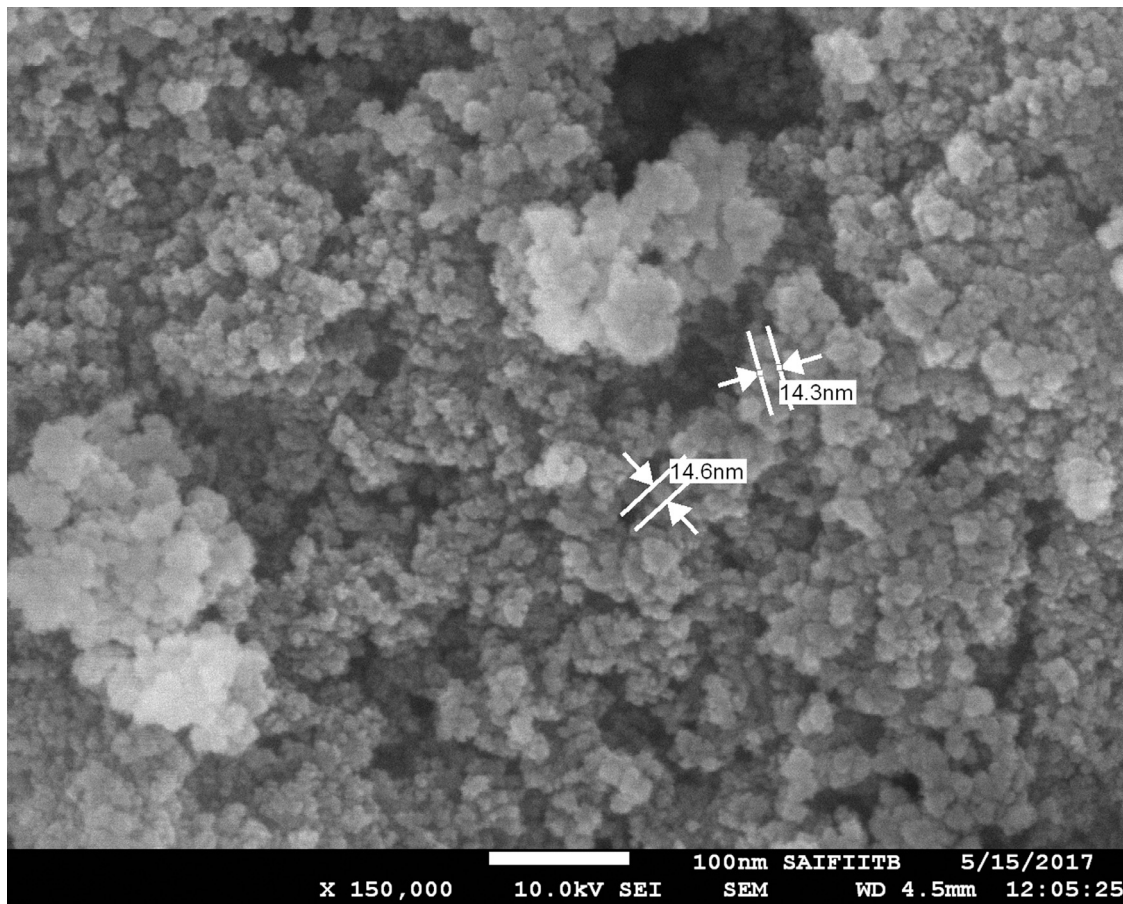


Fig. 5. FEG-SEM image of ZnO/SiO₂ nanocatalyst by palash leaves powder.

Table 5.

Factors and their levels used for two-levels used for two-level fractional factorial design for COD.

| Factor name | Factor Code | Low level (–1) | High level (+1) |
|------------------------------------|-------------|----------------|-----------------|
| pH | A | 9.0 | 11.0 |
| Time (h) | B | 4 | 6 |
| Catalyst loading (gm/L) | C | 1.0 | 1.5 |
| Initial concentration (mg/L) | D | 550 | 275 |
| Temperature (°C) | E | 25 | 30 |
| UV- Intensity (W/cm ²) | Constant | 11 | 11 |

Table 6.

Infrared spectroscopy analysis of ZnO/SiO₂ nanocatalyst by Palash leaves Powder.

| Frequency (cm ⁻¹) | Bond |
|-------------------------------|----------------------------|
| 492.83 | ZnO stretching [18,24] |
| 796.63 | N-H stretching [20,25] |
| 981.80 | Si–O–Si stretching [20,26] |
| 1028.09 | C–N stretching [20,26] |
| 1065.71 | C–O stretching [20,25] |
| 1337.68 | C=O stretching [26] |
| 1524.78 | C–O stretching [15] |
| 1634.73 | N–H stretching [13,15,27] |
| 1764.93 | C=O [13] |
| 2293.44 | O–H stretching [18] |
| 3088.14 | O–H Stretching [13] |
| 3606.04 | O–H Stretching [18] |
| 3739.13 | Si–OH Stretching [26] |

time on percent removal of pollutants, like COD, and acenaphthylene samples were taken and analysed at the various time intervals

such as 0.5 h, 1 h, 2 h 3 h 4 h,5 h,6 h The photocatalytic reaction to treat petroleum refinery effluent was performed in the annular photocatalytic reactor at 25 °C and 30 °C temperature and 6 h as reaction time at different pH. The reaction was performed in the reactor for 6 h' duration and samples were withdrawn from annular reactor periodically in the time interval of 0.5 h, 1 h, 1.5 h, 2 h, 3 h, 4 h, 5 h, and 6 h The synthetic aqueous solution of acenaphthylene was used to find percent removal of PAH by the photocatalytic reaction by HPLC analysis. The petroleum refinery effluent was treated to find percent removal of COD by spectrophotometer. After 6 h, reaction samples were filtered and were analysed to know the residual concentration of pollutant like acenaphthylene (PAH), and COD (mg/L). The concentration of acenaphthylene was found by HPLC (Waters PAH Column 5 μm 4.6 × 250 mm at 27 °C), and COD was found by spectrophotometer. The operative conditions of experiments have been shown in Table 3.

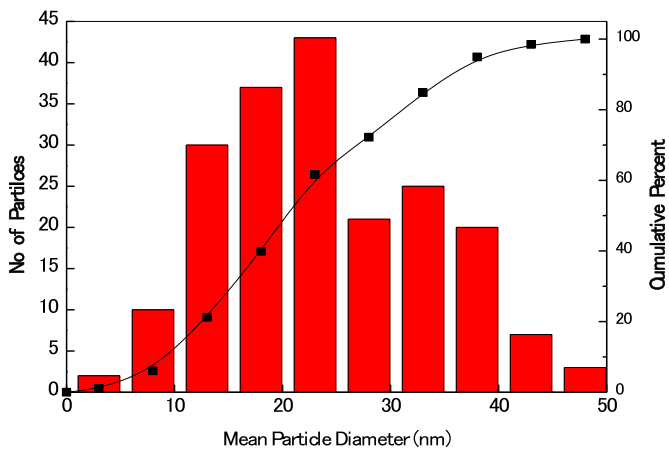


Fig. 6. Calculation of mean particle diameter and Particle size range from FEG-SEM image.

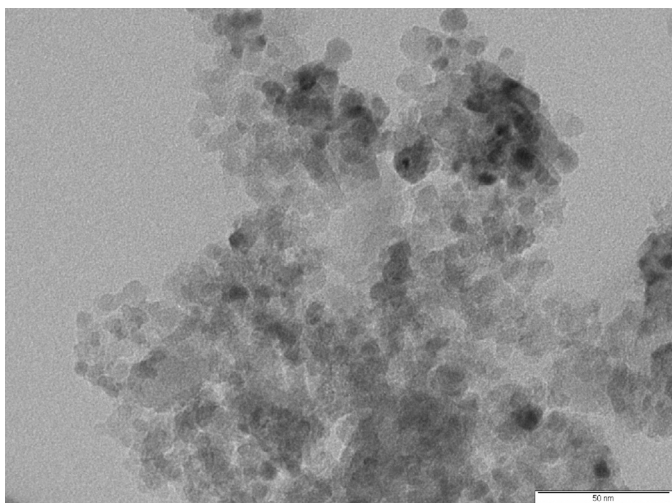


Fig. 7. TEM image of ZnO/SiO₂ nanocatalyst by palash leaves powder.

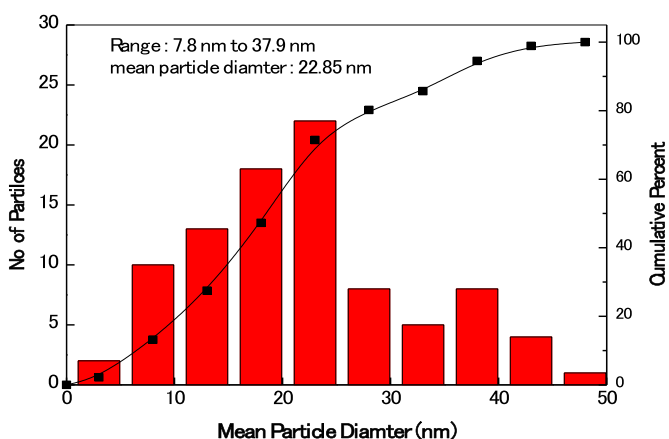


Fig. 8. Calculation of mean particle diameter and Particle size range from FEG-SEM image.

2.6. Photocatalytic annular reactor

This is basically a batch reactor with two coaxial cylinders. The inner cylinder is used for reaction and UV-lamp is placed on the symmetry axis. The total volume of the reactor is 1 L.

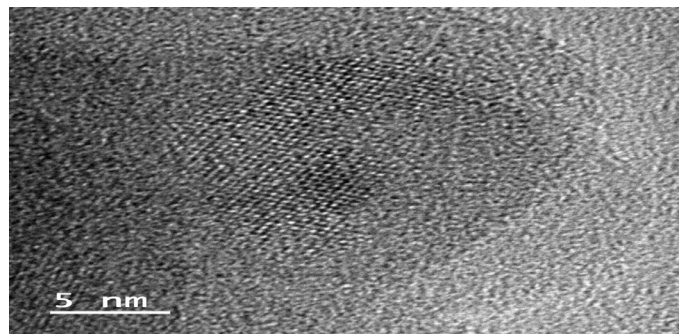


Fig. 9. HR-TEM for single particle of ZnO/SiO₂ nanocatalyst.

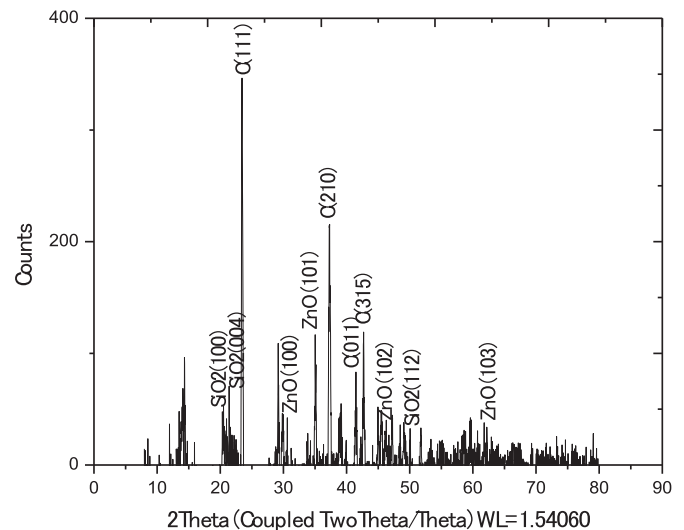


Fig. 10. XRD pattern of ZnO/SiO₂ nanocatalyst synthesized by palash leaves powder.

The outer cylinder is used for water circulation at the maintained temperature inside the reactor. The outer walls of the reactor are designed in this way that they reflect maximum photons emitted by UV-lamp to the reaction medium. Magnetic stirrer has been used at the bottom of the reactor for uniform mixing. For performing this experiment, 0.5 g nanocatalyst was mixed with 500 ml petroleum refinery effluent and the UV-light (11 W/cm²) was started for photocatalytic degradation of acenaphthylene, and COD.

2.7. Photocatalytic degradation studies and kinetic

The amount of the acenaphthylene, COD uptake and percentage removal acenaphthylene, COD were calculated by following Eq. (1) and (2) respectively:

$$q_t = (C_o - C_t) * \frac{V}{M} \quad (1)$$

$$\% \text{ removal} = 100 * (C_o - C_t) \frac{1}{C_o} \quad (2)$$

Where q_t is the removal capacity (COD, acenaphthylene removal by mass unit of the catalyst, mg/g), C_o and C_t are the concentration of COD and acenaphthylene at initial and at time t (mg/L) respectively. M is the catalyst amount (g), and V is the volume of the solution (L). The reaction kinetic was performed by zero-order, first-order, second-order kinetic and intra-particle diffusion model.

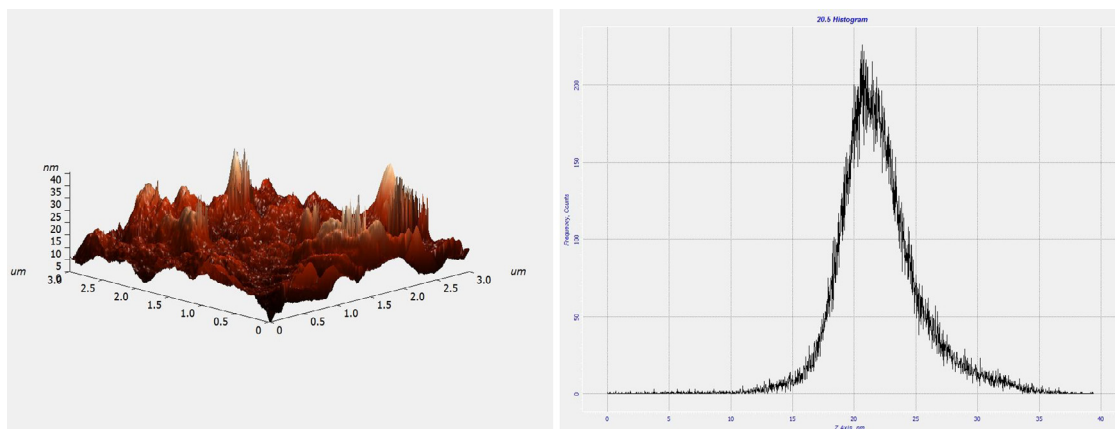


Fig. 11. AFM analysis of ZnO/SiO₂ nanocatalyst synthesized by palash leaves powder.

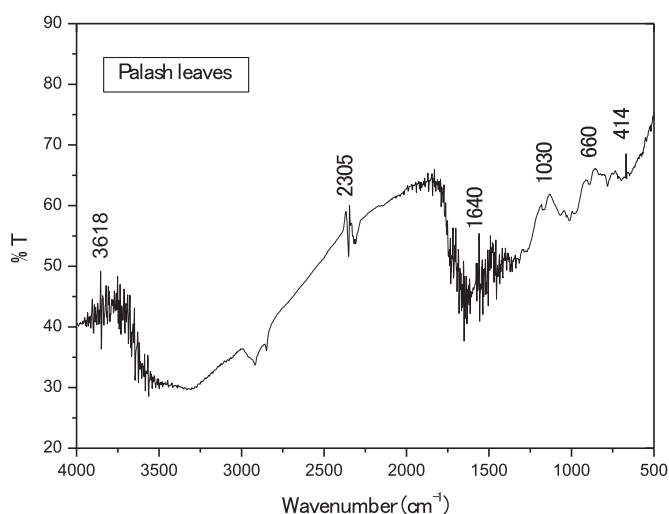


Fig. 12. FTIR analysis of palash leaves powder.

2.8. Theory and calculation

1 mM ZnO aqueous solution of bulk size ZnO powder was used as a precursor for the synthesis of ZnO nanocatalyst. Initially, ZnO was insoluble in water but after adding a few drops of 1 M HCl acid in ZnO solution, a clear solution appeared. ZnO is completely soluble in water after adding HCl due to the decomposing of ZnO into ZnCl₂ and H₂O. Here ZnCl₂ works as a precursor to provide Zn⁺² ions to convert these Zn⁺² ions in nano range with biomolecules present in palash leaves' powder. After bio reduction process, bulk size ZnO was reduced in nano range because palash leaves' powder contains various biomolecules which work here as reducing and stabilizing agents. Mechanism of ZnO/SiO₂ nanocatalyst synthesis by palash leaves' powder has been explained by Bharati and Suresh in their previous work [12]. This is the advantage of using palash leaves' powder as reducing and stabilizing agent since SiO₂ is naturally present in palash leaves.

2.9. Optimization

Optimization was performed by Fractional Factorial Design to know effect of various parameters such as pH, catalyst loading, and initial concentration of pollutants, temperature and time for refinery wastewater treatment for COD removal and for acenaphthylene removal from synthetic aqueous solution.

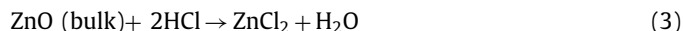
2.9.1. Experimental design

The effects of pH, irradiation time, light intensity ZnO/SiO₂ catalyst loading, and initial COD & acenaphthylene concentration on the efficiency of COD & acenaphthylene photocatalyzed degradation process were investigated. Fractional Factorial design (FFC) was applied in optimization of process parameters in photocatalytic degradation of COD and acenaphthylene under UV light. Two levels for each of the five factors (2^x) were assigned either as low (−1) or high (+1) as shown in Table 4 and Table 5. Eight sets of experimental conditions (2⁵⁻², quarter factorial design, resolution III) were performed in three replicates shown in Table 4 and Table 5. Under UV-light each experiment specified has been performed. The optimum conditions are 225 mg/L initial COD concentration, A (75) % removal of COD removal of petroleum refinery wastewater, and a (73) % removal of acenaphthylene of synthesis aqueous solution was observed under UV-light in 4 h for 50 mg/L initial concentration. Table 4 and Table 5 show Fractional Factorial Design for acenaphthylene and COD respectively.

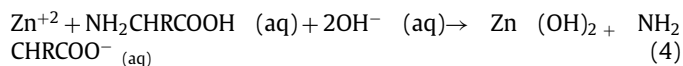
3. Results and discussion

3.1. Mechanism for synthesis of ZnO/SiO₂ nanocatalyst by palash leaves powder

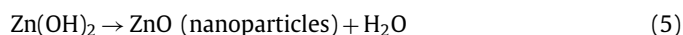
In this experiment 1 mM ZnO aqueous solution was taken ZnO was insoluble in water so some drops of 1 N HCl was added, clear solution of ZnCl₂ got which was used as salt precursor of Zn⁺² ions, than few drops of NaOH was added in ZnO and palash leaves powder reaction at alkaline pH 9.5



When, NaOH was added for reaction at an alkali is medium, the COOH group combines with OH[−] ions from the alkali by loss of H⁺ to form



This reaction is shown for amino acid present in protein biomolecules same reaction will happen for other biomolecules present in palash leaves powder, this amino acid & other functional groups present in biomolecules will be coated with ZnO nanoparticles to work as reducing and stabilizing agent



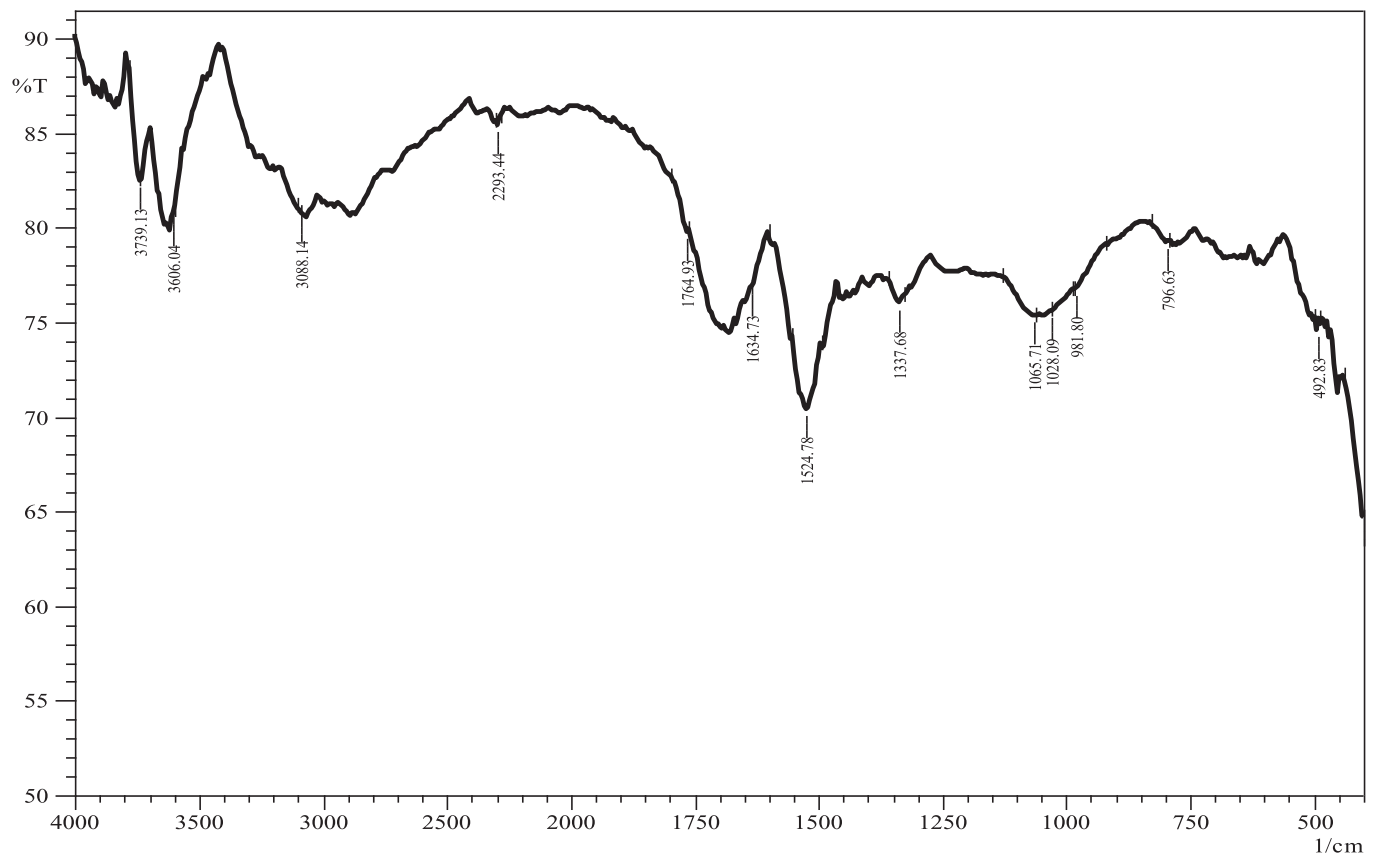


Fig. 13. FTIR analysis of ZnO/SiO₂ nanocatalyst synthesized by palash leaves powder.

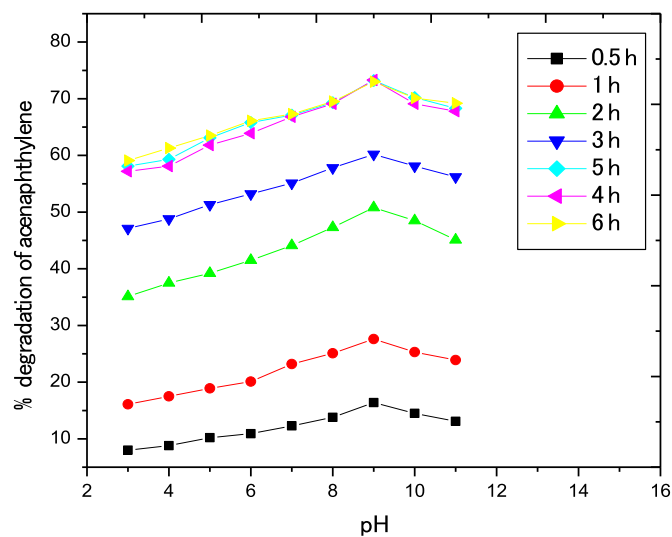


Fig. 14. Effect of pH on % degradation of acenaphthylene at different irradiation times (Catalyst loading = 1 g/L, T = 30 °C).

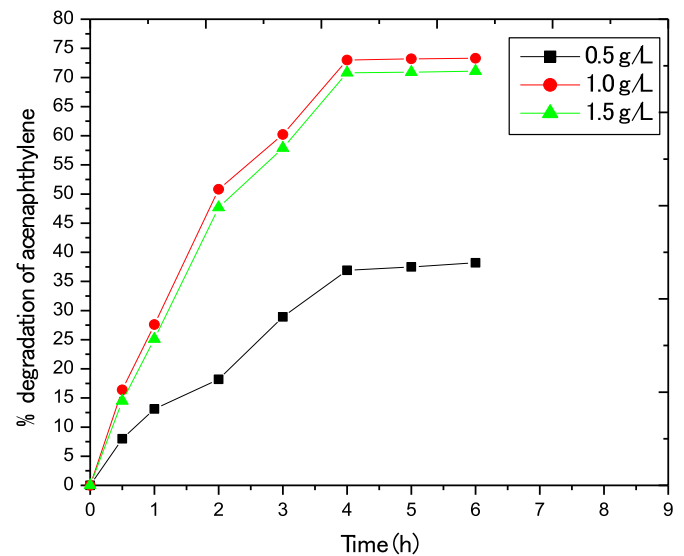


Fig. 15. Effect of the amount of ZnO/SiO₂ on reduction of acenaphthylene at different irradiation times (pH = 9 and T = 30 °C).

SiO₂ was naturally present in palash leaves powder shown by EDX and FTIR of palash leaves powder [13–15].

The mechanism and role of biomolecules present in palash leaves are shown in Fig. 1

3.2. Nanocatalyst synthesis

ZnO/SiO₂ nanocatalyst was synthesized using bio reduction method. Yield and morphology of nanocatalyst, synthesized by this

method, depend on various reaction parameters such as reaction time, light, pH, initial concentration, temperature, mixing speed, the electron donor, and its concentration [11,14–18]. In this experiment, reaction was performed at constant room temperature 24 h Fig. 2 shows the effect of pH on catalyst yield. Fig. 2 shows the effect of the pH yield of synthesized nanocatalyst. Fig. 1 demonstrates that at pH 2, the yield of nanocatalyst was low and it expanded after increment in pH and yield of the catalyst is the most

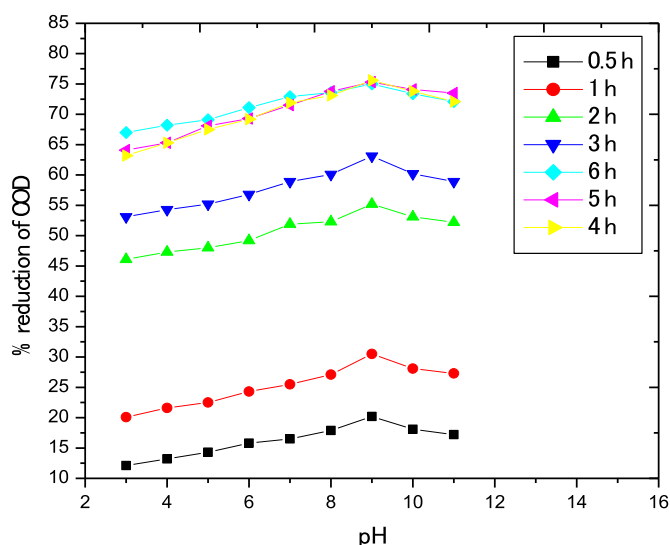


Fig. 16. Effect of pH on % reduction of COD at different irradiation of times (Catalyst loading = 1 g/L, T = 30 °C).

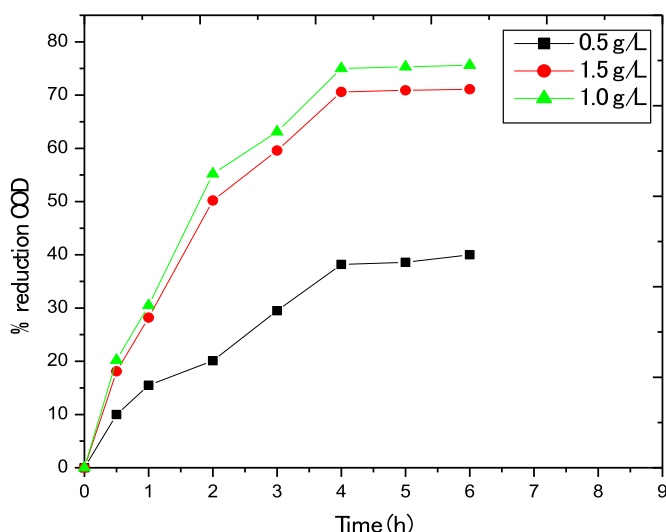


Fig. 17. Effect of the amount of ZnO/SiO₂ on reduction of acenaphthylene at different irradiations time (pH = 9 and T = 30 °C).

elevated at 9.0 pH. After 9.0 pH level, no significant increment was seen in yield of synthesized nanocatalyst through biosynthesis method [28–34].

3.3. Characterization

3.3.1. FEG-SEM and EDX analysis

Fig. 2 EDX spectra of palash leaves powder and shows that Silica in palash leaves powder is 1.48 percent. Fig. 4 shows EDX spectra for synthesized ZnO/SiO₂ nanocatalyst, it is found by EDX analysis that elemental composition of nanocatalyst is C = 47.5%, O = 34.33%, Si = 8.19%, Zn = 4.48%, Re = 1.75%, Mg = 1.71%, Ca = 1.17%, Cu = 0.42%, S = 0.23%, Cl = 0.15%, K = 0.08. EDX spectra shows that strong peaks are found for Si, O, Zn and C in synthesized nanocatalyst so it is confirmed that synthesized nanoparticles are ZnO and SiO₂ [16]. due to the presence of some palash leaves' powder, C is also found with catalyst. Many researches show that carbonaceous nanomaterials enhance photocatalyst activity of catalyst [17].

Fig. 5 shows FEG-SEM image of synthesized ZnO/SiO₂ nanocatalyst. The particle size, shape and surface morphology of the ZnO

Table 7.

Design matrix for 2⁵⁻² for fractional factorial design employed for acenaphthylene photocatalytic degradation.

| S. No. | A | B | C | D | E | % Degradation acenaphthylene Experimental |
|--------|----|----|----|----|----|---|
| 1 | 1 | 1 | 1 | 1 | 1 | 36.3 |
| 2 | 1 | -1 | 1 | -1 | 1 | 68.1 |
| 3 | -1 | -1 | 1 | 1 | -1 | 34.2 |
| 4 | 1 | 1 | -1 | 1 | -1 | 36.1 |
| 5 | 1 | 1 | -1 | 1 | -1 | 36.1 |
| 6 | 1 | -1 | 1 | -1 | 1 | 70.8 |
| 7 | 1 | -1 | -1 | -1 | -1 | 72 |
| 8 | -1 | 1 | -1 | -1 | 1 | 73 |
| 9 | 1 | 1 | 1 | 1 | 1 | 36.1 |
| 10 | -1 | 1 | 1 | -1 | -1 | 69 |
| 11 | -1 | 1 | -1 | -1 | 1 | 73 |
| 12 | 1 | -1 | 1 | -1 | 1 | 67.8 |
| 13 | -1 | -1 | -1 | 1 | 1 | 38.2 |
| 14 | 1 | 1 | 1 | 1 | 1 | 36.1 |
| 15 | -1 | 1 | 1 | -1 | -1 | 70.1 |
| 16 | -1 | -1 | -1 | 1 | 1 | 38.5 |
| 17 | -1 | 1 | 1 | -1 | -1 | 70.1 |
| 18 | 1 | -1 | -1 | -1 | -1 | 68.2 |
| 19 | -1 | -1 | -1 | 1 | 1 | 38.6 |
| 20 | 1 | -1 | -1 | -1 | -1 | 68.5 |
| 21 | -1 | 1 | -1 | -1 | 1 | 73.3 |
| 22 | -1 | -1 | 1 | 1 | -1 | 36.7 |
| 23 | -1 | -1 | 1 | 1 | -1 | 36.6 |
| 24 | 1 | 1 | -1 | 1 | -1 | 38.3 |

/SiO₂ nanocatalyst were analyzed by FEG-SEM image. By FEG-SEM image, it is analyzed that synthesized nanoparticles are in nanorange [16]. FEG-SEM image shows agglomeration at some spot in nanocatalyst sample due to presence of large particles of C. From FEG-SEM, image histogram is prepared and by the histogram graph, particle size range and mean particle diameter are calculated as shown in Fig. 6. The particle size ranges from 8 to 40 nm and mean particle diameter is 20 nm. It has been found that nanoparticles are spherical in shape from FEG-SEM Image [18].

3.3.2. TEM analysis

Fig. 7 shows TEM image and Fig. 9 shows HR-TEM image for single particles and Fig. 8 shows its histogram graph. From TEM image, particle size and mean particle diameter are calculated and particle size range is found from 7.83 nm to 37.9944 nm and mean particle diameter is 22.85 nm. Similar kind of result is obtained from FEG-SEM analysis. Thus, it is confirmed that synthesized nanocatalyst are in nanorange of 8 to 20 nm [18,19].

3.3.3. XRD analysis

Fig. 10 shows XRD analysis of synthesized ZnO/SiO₂ nanocatalyst. From XRD analysis, phase identification is done. XRD result shows prominent peaks of Carbon (C) and weak and clear peaks of ZnO and SiO₂ nanocatalyst [17]. XRD peaks confirmed the presence of ZnO corresponding to PDF No. 800,075. Lattice Constant (parameters) a and c were calculated to be 3.25 Å and 5.209 Å respectively [16,18]. From XRD, results show that crystal structure of ZnO is found hexagonal; it is more stable form in the environment. XRD peaks confirmed the presence SiO₂ corresponding PDF No. 861,630 and 860,681 [18,14]. Particles mean diameter is calculated by XRD results with the help of Debye Sherrer's equation.

$$D = 0.94\lambda / B\cos\theta \quad (6)$$

From above equation, it is confirmed that mean particle diameter of synthesized nanocatalyst is 20.2 nm.

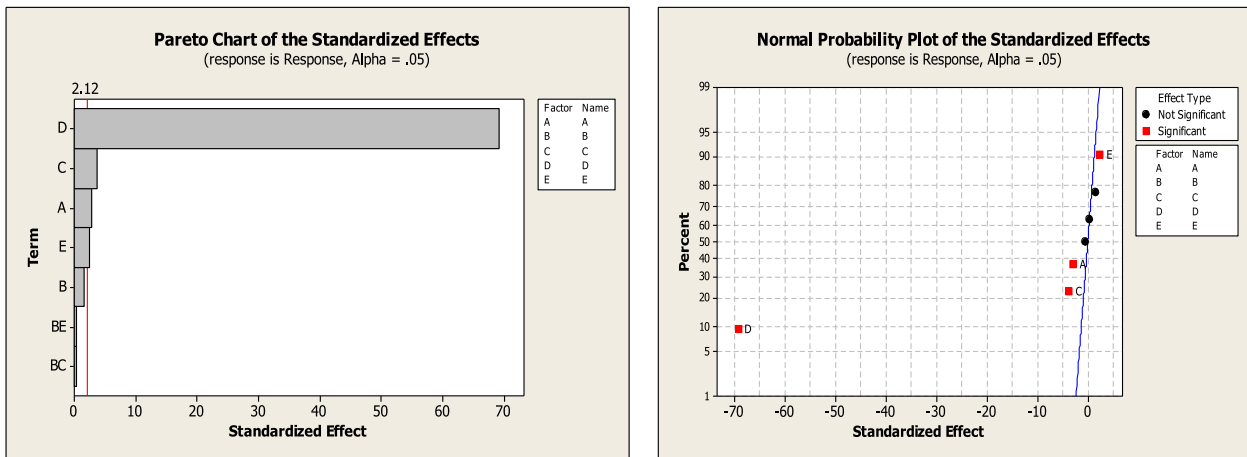


Fig. 18. (a) Pareto Chart of the standardized effects of single and interaction factors on % acenaphthylene photodegradation. (b) Normal plot of the standardized effect of single and interaction factors on % acenaphthylene photodegradation.

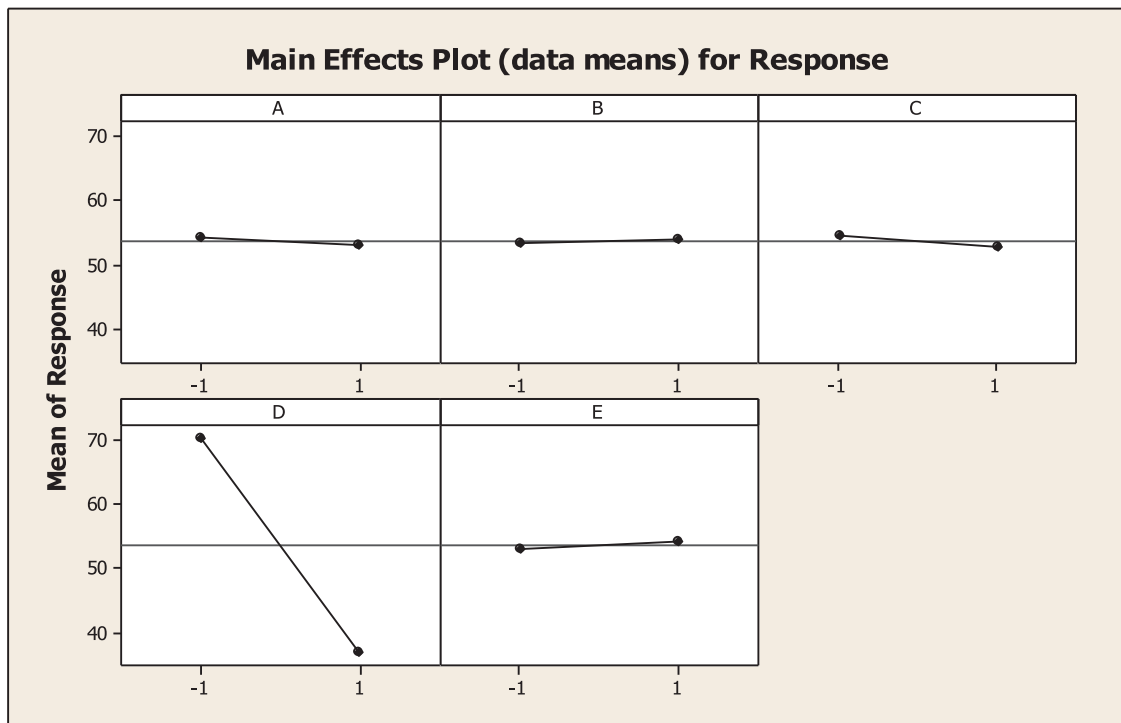


Fig. 19. Plot for effects of various parameters on % removal of acenaphthylene.

3.3.4. AFM analysis

Fig. 11 Shows AFM analysis of ZnO/SiO₂ nanocatalyst synthesized by palash leaves powder and from histogram images it is confirmed that particles size range is 7 nm to 38 nm.

3.3.5. FTIR analysis

Fig. 12 shows FTIR analysis palash leaves powder to find functional group present in it and found that transmittance peak at 414 cm⁻¹ for Si-O stretching, peak at 3618 cm⁻¹ for O-H stretching for phenolic group, peak at 660 cm⁻¹ for N-H stretching for amines, peak at 1030 cm⁻¹ for C-N stretching for aliphatic amines, peak at 1310 cm⁻¹ for C-O stretching for alcohols and peaks at 1640 cm⁻¹ for N-H stretching for primary amines are due to functional groups present in palash leaves because it contain protein, Carbohydrate and flavonoids biomolecules. Fig. 13 shows FTIR analysis of ZnO/SiO₂ nanocatalyst. From FTIR analysis of Fig. 13, functional groups for corresponding IR frequencies are shown in

Table. 6 for synthesized ZnO/SiO₂ nanocatalyst. From FTIR analysis, presence of various functional groups is identified in a sample of synthesized nanocatalyst. These functional groups work as capping and stabilizing agents. FTIR result is also showing stretching for Si-O-Si and in Zn-O, thus it has been confirmed that synthesized nanocatalyst ZnO/SiO₂ nanocomposite. From FTIR image, it can be said that ZnO stretching is found at IR frequency 492.83 and 1634.73 [13,18,20]. And for SiO₂, IR, frequency is found at 981.80 1028.09 and 1065.71 [20].

3.4. Treatment of petroleum refinery effluent by ZnO/SiO₂ nanocatalyst

The percent removals of pollutant, by photocatalytic reaction, depend on various factors like catalyst load, pH, time, UV-light intensity, temperature and initial concentration of pollutants [4]. The effectiveness of catalytic reaction is analyzed by changing various

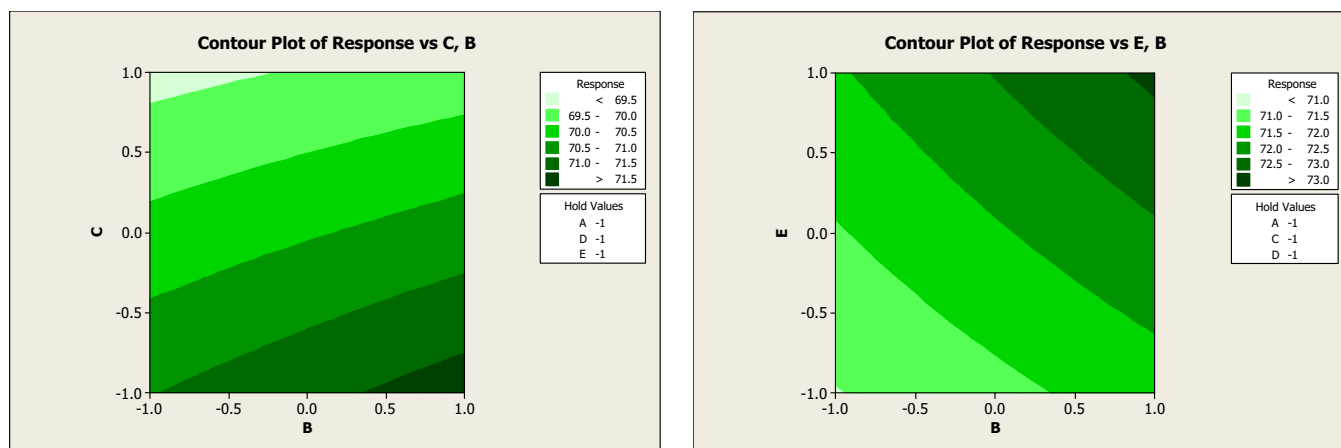


Fig. 20. (a) Contour plot for % acenaphthylene photodegradation versus a time and catalyst load (hold values: UV light intensity=11 W/cm², pH=9, and Temperature 30 °C, initial concentration =50 mg/L). (b) Counter plot for % acenaphthylene photocatalytic degradation versus a time and Temperature (hold values: initial concentration=50.00 mg/L, pH=9, and catalyst loading=1.0 g/L).

Table 8.

Design matrix for 2⁵⁻² for fractional factorial design employed for COD photocatalytic degradation.

| S. No. | A | B | C | D | E | % reduction of COD experimental |
|--------|----|----|----|----|----|---------------------------------|
| 1 | 1 | 1 | 1 | 1 | 1 | 45.1 |
| 2 | 1 | -1 | 1 | -1 | 1 | 65.1 |
| 3 | 1 | -1 | -1 | -1 | -1 | 71.5 |
| 4 | -1 | 1 | -1 | -1 | 1 | 75.5 |
| 5 | -1 | -1 | -1 | 1 | 1 | 40.0 |
| 6 | -1 | -1 | 1 | 1 | -1 | 16 |
| 7 | -1 | 1 | -1 | -1 | 1 | 75.6 |
| 8 | -1 | -1 | -1 | 1 | 1 | 35.0 |
| 9 | 1 | 1 | -1 | 1 | -1 | 35.1 |
| 10 | 1 | -1 | -1 | -1 | -1 | 70.2 |
| 11 | -1 | 1 | -1 | -1 | 1 | 75.5 |
| 12 | 1 | -1 | 1 | -1 | 1 | 60.3 |
| 13 | -1 | -1 | 1 | 1 | -1 | 75.1 |
| 14 | 1 | -1 | -1 | -1 | -1 | 70.2 |
| 15 | -1 | 1 | 1 | -1 | -1 | 72.4 |
| 16 | -1 | 1 | 1 | -1 | -1 | 58.5 |
| 17 | 1 | 1 | 1 | 1 | 1 | 28.4 |
| 18 | -1 | -1 | -1 | 1 | 1 | 60.0 |
| 19 | 1 | 1 | -1 | 1 | -1 | 45.2 |
| 20 | 1 | -1 | 1 | -1 | 1 | 70.6 |
| 21 | -1 | 1 | 1 | -1 | -1 | 67.4 |
| 22 | 1 | 1 | 1 | 1 | 1 | 47.6 |
| 23 | -1 | -1 | 1 | 1 | -1 | 37.9 |
| 24 | 1 | 1 | -1 | 1 | -1 | 49.0 |

Table 9.

Optimum condition.

| Parameter (Unit) | Value |
|---|-------|
| Initial COD concentration (mg/L) | 225 |
| Initial acenaphthylene concentration (mg/L) | 50 |
| Catalyst loading (g catalyst/L solution) | 1.0 |
| Solution pH | 9 |
| Temperature (°C) | 30 |
| UV intensity (W/m ²) | 11 |

factors and determined optimum values for corresponding factors. The photocatalytic reaction is performed under UV-light source for better results. 100 mg/L, 75 mg/L and 50 mg/L initial concentration of acenaphthylene was taken for photocatalytic degradation and their concentrations were determined by HPLC analysis. COD was reduced from petroleum refinery effluent and concentration was determined by spectrophotometer the initial concentration of COD

was 550 mg/L, 375 mg/L and 275 mg/L was measured for photocatalytic degradation.

3.4.1. Effect of time

Figs. 14 and 16 show percent removal of acenaphthylene and COD with time and pH. And it shows from these graphs that initially % reduction increase with increasing time fastly but after 4 h reaction time catalyst gets saturated and no significance increase occurred so the optimum time is 4 h

3.4.2. Effect of catalyst load

The effect of the amount of ZnO/SiO₂ nanocatalyst on degradation of acenaphthylene and COD is shown in Figs. 15 and 17 respectively. The photocatalytic degradation efficiency increases with increase in the amount of photocatalyst until about 1 g/L of the catalyst and then decreases mildly. The reason of this perception is thought to be the way that increasing the concentration of the catalyst cause an increase in the reaction rate, not just as a result of an increase of the active site of the catalyst but also because of an increase in the hydroxyl radical generation; however, on the other hand, when enough ZnO/SiO₂ is present in the suspension for pollutants molecules, the additional higher quantities of it would not have more effect on the degradation efficiency. Then again, an expanded haziness of the suspension achieved as a results of excess of ZnO/SiO₂ particles [10,11].

3.4.3. Effect of pH on percent removal of pollutants

pH is one of the variables impacting the rate of degradation of some organic compounds in the photocatalytic process. It is likewise an essential working parameter in wastewater treatments. Figs.14 and 16 shows the photocatalytic degradation of acenaphthylene and COD at different pH values. The most appropriate significant variation is within the pH range of 9–11. At pH 3 to 8 protonation takes place and the protonated products are more stable under UV-radiation than its main structure. At pH 3 to 8 the catalyst surface is positively charged leading to a lower level of degradation. At pH 9, there are significantly higher molecules in their non-protonated form providing higher level of adsorption into catalyst surface and then degradation to be favored. It is important that the formation of hydroxyl radicals in acidic solutions and in the presence of oxygen assists the degradation of substrate. In the acidic media, the catalyst surface is positively charged. In the alkaline media the catalyst surface is negatively charged. The COD and, acenaphthylene molecules lose the proton under these conditions, and it increases low tendency to be adsorbed onto the cat-

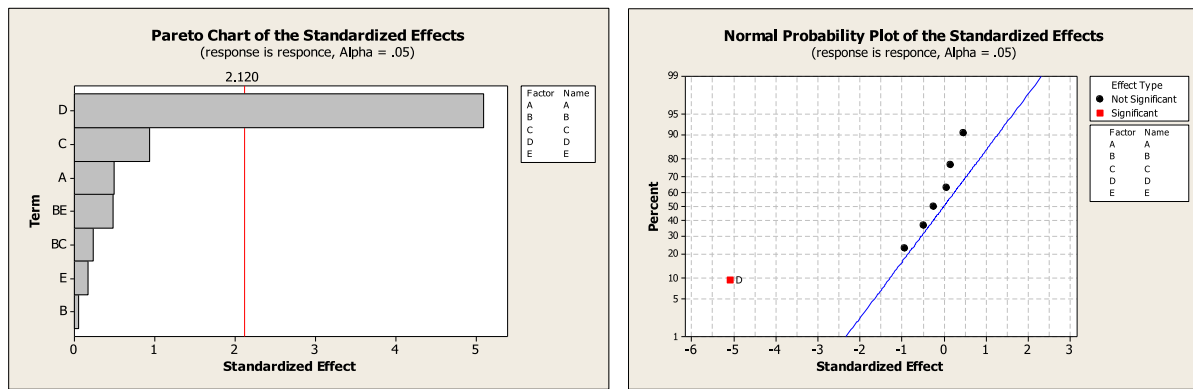


Fig. 21. (a) Pareto chart of the standardized effects of single and interaction factors on % COD photodegradation. (b) Normal plot of the standardized effect of single and interaction factors on % COD photodegradation.

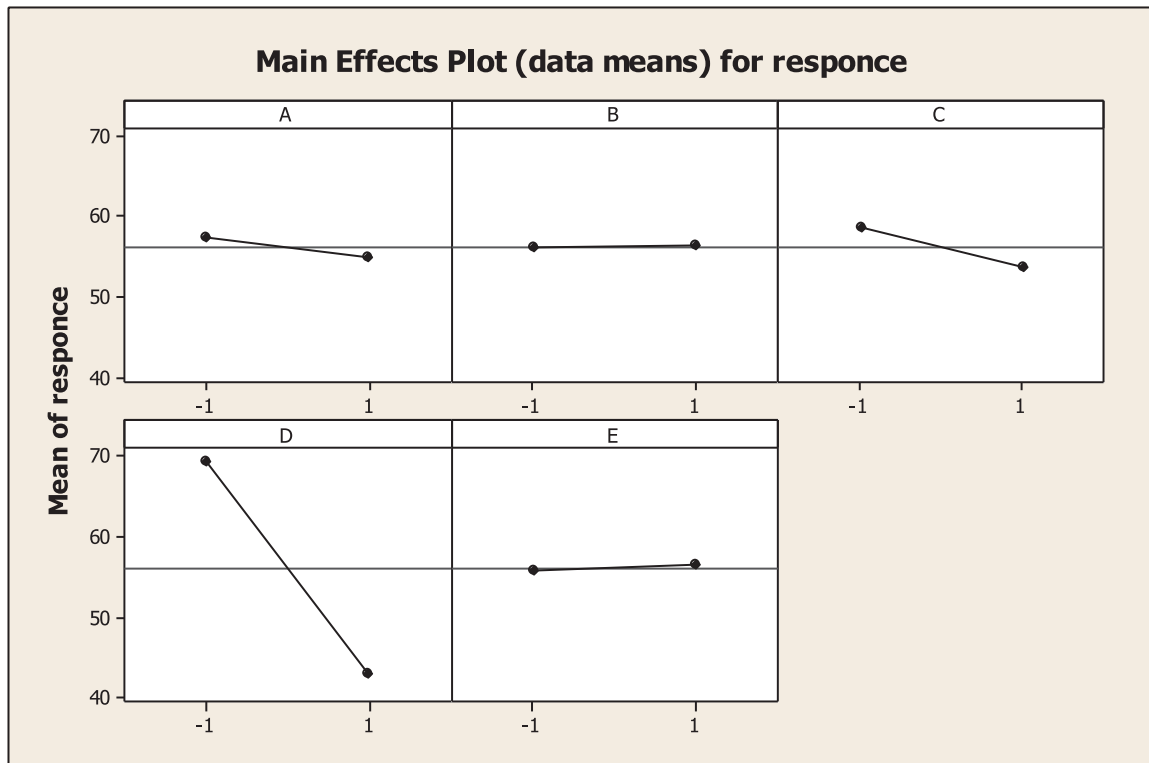


Fig. 22. Plot for effects of various parameters on % removal of COD.

alyst surface. Because, the difference between COD and acenaphthylene degradation efficiency under the pH 3–8 and 10–11 than 9, after 4 h the 9 pH was chosen as an optimum pH value and the experiments was followed under this pH. So the optimum pH for the reaction is obtained from Figs. 14 and 16 for acenaphthylene and COD respectively.

3.4.4. Effect of temperature

In the range 25 to 30 °C, low upgrades in the COD, acenaphthylene removal were observed which must be because of the low activation energy of photocatalytic reaction. At these temperature range photocatalysis is not very much temperature dependent. However, an expansion in temperature helps the reaction to compete more efficiency with the recombination of valance band hole and conduction band electron. On the other hand, an expansion in temperature diminishes the dissolvability of oxygen in water which is not desirable. Temperature higher than 30 °C will bring about significant evaporation of the solution during the experi-

ments. Since the difference between the degradation efficiency of COD and acenaphthylene in the temperature range 25–30 °C, the ambient temperature (25 °C) was picked as the most reasonable temperature esteem without the need to direct the temperature.

3.4.5. Effect of initial concentration of pollutants

The COD and acenaphthylene removal decreases as the initial concentration of COD and acenaphthylene, initial solution pH increases after 9 pH. As the initial concentration of pollutants increases, the equilibrium adsorption of pollutants on the catalyst active sites also increase, hence competitive adsorption of ·OH on the same site decrease. This implies a lower development rate of ·OH radical responsible for pollutants degradation. Additionally as the initial dye concentration increases, the way length of photons emerging the solution decreases, which result in lower photon adsorption on catalyst particles, and therefore bring down photocatalytic reaction rates.

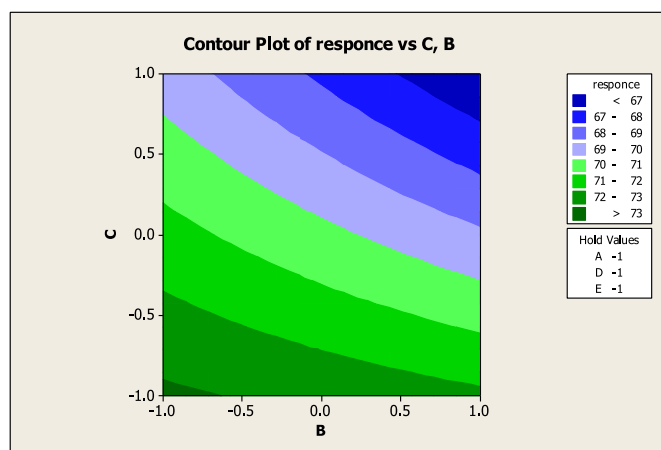


Fig. 23. (a) Contour plot for % COD photodegradation versus a time and catalyst load (hold values: UV light intensity=11 W/cm², pH=9, and Temperature 30 °C, initial concentration =50 mg/L). (b) Counter plot for % acenaphthylene photocatalytic degradation versus a time and Temperature (hold values: initial concentration=50.00 mg/L, pH=9, and catalyst loading=1.0 g/L).

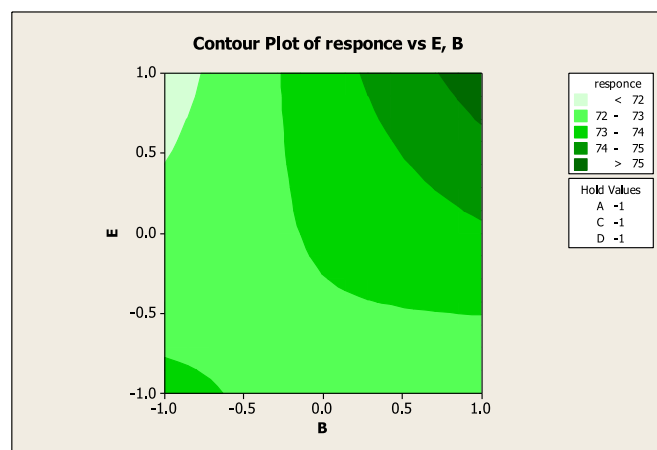


Fig. 23. Continued

3.5. Optimization results analysis

Analysis of the fractional factorial design results was done at 95% confidence level ($p < 0.05$) using the % degradation as the response factor. Pareto graph was used to reach conclusions on the relative significance of the studied factors as well as the interactions between them while the direction of effects was obtained from the normal plot of the standardized effects.

A positive effect indicates that the studied response increases in the presence of high levels of these variables, while negative effect indicates that the response increases in the presence of low levels of these variables, within the studied range. Fractional Factorial design matrix has been shown for acenaphthylene in Table 7 and for COD in Table 8. Acenaphthylene and COD can be calculated from Fractional Factorial design by Regression Eqs. (8) and (9) respectively [10,11].

The regression equation is:

$$\begin{aligned} (\% \text{degradation of acenaphthylene}) = & 53.57 - 0.70A + 0.39B \\ & - 0.91C - 16.75D + 0.58E - 0.10BC + 0.10BE \end{aligned} \quad (8)$$

The regression equation is:

$$\begin{aligned} \% \text{reduction of COD} = & 56.13 - 1.27A + 0.14B - 2.43C \\ & - 13.27D + 0.42E - 0.61BC + 1.25BE \end{aligned} \quad (9)$$

UV light intensity is constant in this experiment. Fig. 18(a) and (b) for acenaphthylene and 21 (a) and (b) for COD removal indicates Pareto Chart of the standardized effect of single and interaction factors. Initial concentration of acenaphthylene (D) was found to have the most significant impact with a negative effect. On the other hand, the significant interaction terms were as follows: irradiation time – reaction temperature (BE), with a positive effect, and irradiation time – catalyst loading (BC), with a negative effect as appeared in Figs. 19 and 20, (a) and (b) for acenaphthylene and 22 and 23, (a) and (b) for COD. It could be concluded from these results that:

(i) Treatment of samples containing low concentration of COD and acenaphthylene should require and reduced pH, catalyst loading. And increased temperature has positive effect on % removal of COD and acenaphthylene [10,11]. At high COD and acenaphthylene concentration levels, the active sites of ZnO/SiO₂ get soaked and more photons are retained leading to a decline in the efficiency of photodegradation of COD and acenaphthylene.

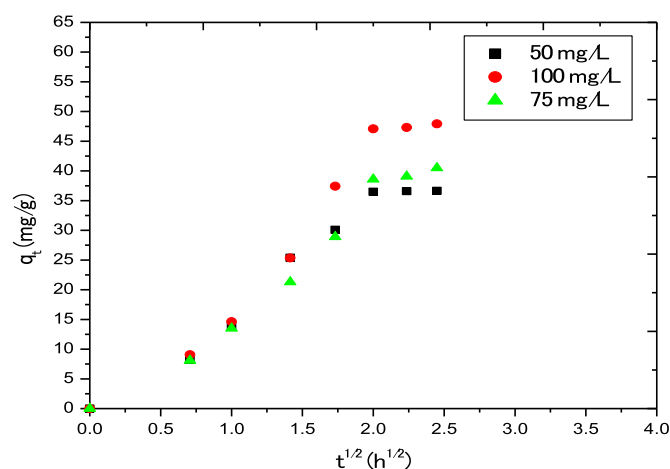


Fig. 24. Plot for intra-particle diffusion of acenaphthylene at various initial concentrations.

- (ii) ZnO/SiO₂ nanocatalyst loading did not significantly influence the photodegradation procedure. This demonstrated that the photocatalytic system had achieved a steady state over the range of 1.0 g/L. When all is said and done, expanding ZnO/SiO₂ below the steady state increases photocatalysis because of the expansion of the available active site. Further addition of the catalyst has been reported to decrease the photocatalytic efficiency because of low light entrance and agglomeration of ZnO/SiO₂ nanocatalyst.
- (iii) It ought to be noticed that the non-noteworthy impact of pH on the photocatalytic performance of ZnO/SiO₂ was in agreement with the theoretical understanding of the catalyst behavior of ZnO/SiO₂ talked about prior.

3.6. Kinetic study

The kinetic study was performed for acenaphthylene and COD to know the mechanism of the rate of photocatalytic reaction. The experimental statistics of photocatalytic reaction for acenaphthylene and COD were fitted in different kinetic models. The R², K, normalized deviation (ND) and normalized standard deviation (NSD) Value for COD removal for zero-order, first-order and Second-order and for intra-particle diffusion were found and have been shown in Table 10. Plot for intra-particle diffusion for acenaphthylene and COD at different initial concentration have been shown in Figs. 24 and 25 respectively [21,22].

Table 10.
Kinetic modeling for different model at different initial concentration.

| S. No. | Kinetic model | Model parameter | Value for COD reduction | Value for acenaphthylene degradation |
|--------|---|-----------------|-------------------------|--------------------------------------|
| 1. | Zero-order kinetic models $\frac{d}{dt}(C_t) = K C_t$ | R ² | .9803 | .9802 |
| | | K | 92.08 | 15.09 |
| | | ND | 5.09 | 5.06 |
| | | NSD | 9.87 | 7.89 |
| 2. | First-order kinetic model $\ln\left(\frac{C_0}{C_t}\right) = K t$ | R ² | 0.986 | 0.9826 |
| | | K | 92.98 | 16.01 |
| | | ND | 3.08 | 5.078 |
| | | NSD | 6.07 | 9.86 |
| 3. | Second-order kinetic model $\frac{1}{(C_t)} = K t + \frac{1}{C_0}$ | R ² | 0.985 | 0.989 |
| | | K | 93.98 | 20.65 |
| | | ND | 3.98 | 4.99 |
| | | NSD | 7.89 | 8.97 |
| 4. | Intra-Particle Diffusion Model $q_t = K t^{1/2} + C$ | R ² | 0.982 | 0.9864 |
| | | K | 94.07 | 22.46 |
| | | ND | 4.5003 | 3.456 |
| | | NSD | 5.0012 | 8.456 |

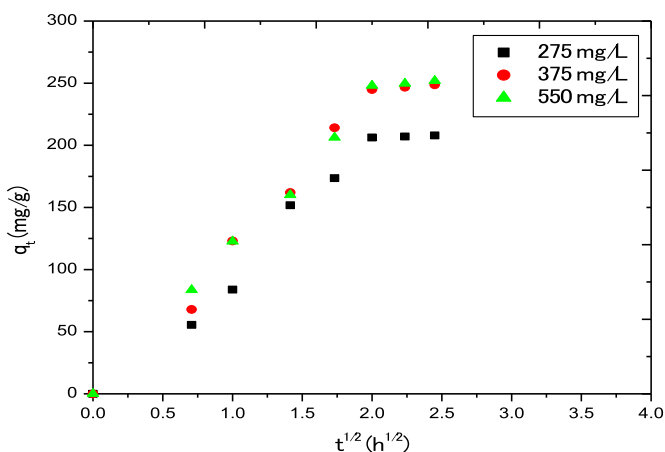


Fig. 25. Plot for intra-particle diffusion of COD at various initial concentrations.

4. Conclusions

The present work of biosynthesis of ZnO/SiO₂ nanocatalyst by palash leaves powder is green synthesis route. This method is rapid and eco-friendly. In this method, Palash leaves' Powder is used as reducing and stabilizing agent to synthesized ZnO/SiO₂ nanocatalyst in place of chemicals so it is an eco-friendly and nontoxic method. From EDX and XRD analysis, it is confirmed that palash leaves contain SiO₂ naturally which increases photocatalytic effectiveness of nanocatalyst. EDX results also show that other metals ions are also present naturally in Palash leaves which increase activity of nanocatalyst. From FEG-SEM image, TEM and XRD particle size and mean particle diameter of nanocatalyst were calculated and they have been found in nano range. The mean particle diameter is 20 nm and particles are in 8 nm to 40 nm range. The EDX and XRD results confirmed that particles are ZnO/SiO₂ nanocatalyst. FTIR results show stretching for ZnO and SiO₂ and for various functional groups which work as capping and stabilizing agents for ZnO/SiO₂ nanocatalyst. The optimum photocatalytic degradation acenaphthylene, and chemical Oxygen Demand is 73%, and 75% respectively at 4 h as reaction time, 30 °C as reaction temperature and 1 g/L dose of ZnO/SiO₂ nanocatalyst.

Conflict of interest

The authors declare no conflict of interest.

Acknowledgements

This work is financially supported by MHRD Government of India and MANIT, Bhopal. Authors deeply acknowledge SAIF, IIT Mumbai and North Maharashtra University Jalgaon for providing characterization facilities for analysis of synthesized nanocatalyst.

References

- [1] S.V. Hegde, G.R. Hegde, S. Mannur, S.S. Poti, Pharmacognostical studies on *Butea monosperma* (Lam.) Taub (Fabaceae) flower, *Int. J. Pharm. Phytopharmacol. Res.* 4 (1) (2014) 34–36.
- [2] S.B. Dhull, P. Kaur, S. S.Purewal, Phytochemical analysis, phenolic compounds, condensed tannin content and antioxidant potential in Marwa (*Origanum majorana*) seed extracts, *Resour. Effic. Technol.* 2 (1) (2016) 168–174.
- [3] G. Sandmann, H. Dietz, W. Plieth, Preparation of silver nanoparticles on ITO surfaces by a double-pulse method, *J. Electroanal. Chem.* 491 (1) (2000) 78–86.
- [4] C.H. Bae, S.H. Nam, S.M. Park, Formation of silver nanoparticles by laser ablation of a silver target in NaCl solution, *Appl. Surf. Sci.* 197–198 (1) (2002) 628–634.
- [5] G. Thooyavan, G. J. Karthikeyan, Phytochemical profiling and GC-MS analysis of *Butea monosperma* seed methanol extract, *J. Pharmacognosy Phytochem.* 5 (5) (2016) 152–157.
- [6] A.K. Mittal, Y. Chisti, U.C. Banerjee, Synthesis of metallic nanoparticles using plant extracts, *Biotechnol. Adv.* 31 (2) (2013) 346–356.
- [7] M. Kokate, K. Garadkar, A. Gole, Zinc-oxide-silica-silver nanocomposite: Unique one-pot synthesis and enhanced catalytic and anti-bacterial performance, *J. Colloid Interface Sci.* 483 (2016) 249–260.
- [8] R. Raliya, J.C. Tarafdar, ZnO nanoparticle biosynthesis and its effect on phosphorous-mobilizing enzyme secretion and gum contents in Clusterbean (*Cyamopsis tetragonoloba* L.), *Agricultural Res.* 2.1 (2013) 48–57.
- [9] I.M. El-Nahhal, J.K. Salem, S. Kuhn, T. Hammad, R. Hempelmann, S.A. Bhaisi, Synthesis & characterization of silica coated and functionalized silica coated zinc oxide nanomaterials, *Powder Technology* 287 (2016) 439–446.
- [10] A.H. Nadim, M.A. Al-Ghobashy, M. Nebsen, M.A. Shehata, Optimization of photocatalytic degradation of meloxicam using titanium dioxide nanoparticles: application to pharmaceutical wastewater analysis, treatment, and cleaning validation, *Environ. Sci. Pollut. Res. Int.* 22 (20) (2015) 15516–15525, doi:10.1007/s11356-015-4713-2.
- [11] J. Saien, S. Khezrianjoo, Degradation of the fungicide carbendazim in aqueous solutions with UV/TiO₂ process: Optimization, kinetics and toxicity studies, *J. Hazardous Mater.* 157 (2008) 269–276.
- [12] R. Bharati, S. Suresh, Green synthesis of ZnO/SiO₂ nanocatalyst with palash leaves extract for treatment of petroleum refinery effluent, *Adv. Mater. Proc.* 1 (1) (2016) 979–983, doi:10.5185/amp.2016/101.
- [13] H. Kumar, R. Rani, Structural and optical characterization of ZnO nanoparticles synthesized by microemulsion route, *Int. Lett. Chem. Phys. Astron.* 14 (2013) 26–36.
- [14] K.S. Kavitha, S. Baker, D. Rakhith, H.U. Kavitha, Rao H.C. Yashwantha, B.P. Harini, S. Satish, Plants as green source towards synthesis of nanoparticles, *Int. J. Biol. Sci.* 2 (6) (2013) 66–76.
- [15] M.I. Khalil, M.A. Qunaibit, A.M.A. Zahem, J.P. Labis, Synthesis and characterization of ZnO nanoparticles by thermal decomposition of a curcumin zinc complex, *Arabian J. Chem.* 7 (2014) 1178–1184.
- [16] R.N. Gayen, K. Sarkar, S. Hussain, R. Bhar, A.K. al, ZnO films prepared by modified Sol-gel technique, *Indian J. Pure Appl. Phys.* 49 (1) (2011) 470–477.
- [17] R. Leary, A. Westwood, Carbonaceous nano materials for the enhancement of TiO₂ photocatalysis, *Carbon* 49 (2011) 741–772.

- [18] Z.R. Khan, Khan M.S., M. Zulfequar, M.S. Khan, Optical and structural properties of ZnO thin films fabricated by Sol-gel method, *Mater. Sci. Appl* 2 (1) (2011) 340–345.
- [19] K. Nivedh, S.K.R. Namasivayam, A.N. Nishanth, Effect of functionalization of polymeric nanoparticles incorporated with whole attenuated rabies virus antigen on sustained release and efficacy, *Resour.-Efficient Technol.* 2 (1) (2016) S25–S38, doi:10.1016/j.refit.2016.10.007.
- [20] A.A. Magda, F.A. Hesham, M.A. Hesham, A.M.E. Soliman, AbdEl Rahman, Ahmed, I. Abd-Elhamid, Preparation and characterization of silica nanoparticles by wet mechanical attrition of white and yellow sand, *J. Nanomed. Nanotechnol.* 4 (6) (2013) 2–14.
- [21] M. Ganesapillai, P. Simha, The rationale for alternative fertilization: equilibrium isotherm, kinetics and mass transfer analysis for urea-nitrogen adsorption from cow urine, *Resour.-Efficient Technol.* 1 (2015) 90–97.
- [22] P. Simha, A. Yadav, D. Pinjari, A.B. Pandit, On the behaviour, mechanistic modelling and interaction of biochar and crop fertilizers in aqueous solutions, *Resour.-Efficient Technol.* 2 (2016) 133–142.
- [23] L. Yu, M. Han, F. He, A review of treating oily wastewater, *Arabian J. Chem.* 5 (1) (2016) 1–10.
- [24] E-S.Z. El-Ashtouky, Y.A. El-Taweel, O. Abdelwahab, E.M. Nassef, Treatment of petroleum refinery effluent containing phenolic compounds by electrocoagulation using a fixed bed electrochemical reactor, *Int. J. Electrochem. Sci* 8 (2013) 1534–1550.
- [25] A.M. Putz, M.V. Putz, Spectral inverse quantum (Spectral-IQ) method for modeling mesoporous systems: application on silica films by FTIR, *Int J. of Mol. Sci.* 13 (1) (2012) 15925–15941.
- [26] A. Mourhly, M. Khachani, A. El Hamidi, M. Kacimi, M. Halim, S. Arsalan, The synthesis and characterization of low-cost mesoporous silica SiO₂ from local pumice rock, *Nanomater. Nanotechnol.* 35 (5) (2015) 4–6.
- [27] R.N. Gayen, K. Sarkar, S. Hussain, R. Bhar, A.K. Pal, ZnO films prepared by modified Sol-gel technique, *Indian J. Pure Appl. Phys.* 49 (1) (2011) 470–477.
- [28] S. Ahmed, M. Ahmad, B.L. Swami, S. Ikram, A review on plants extract mediated synthesis of silver nanoparticles for antimicrobial applications, a green expertise, *J. Adv. Res.* 7 (1) (2016) 17–28.
- [29] G. Sangeetha, S. Rajeshwari, R. Venkatesh, Green synthesis of Zinc oxide nanoparticles by aloe barbadensis miller leaf extract: structure and optical properties, *Mater. Res. Bull.* 46 (1) (2011) 2560–2566.
- [30] J.Y. Song, B.S. Kim, Biological synthesis of bimetallic Au/Ag nanoparticles using Persimmon (*Diopyros kaki*) leaf extract, *Korean J. ChemEng* 25 (1) (2008) 808–811.
- [31] K.D. Arunachalam, S.K. Annamalai, S. Hari, One-step green synthesis and characterization of leaf extract-mediated biocompatible silver and gold nanoparticles from *Memecylonumbellatum*, *Int. J. Nanomedicine* 8 (1) (2013) 1307–1315.
- [32] G.P. Gaddekar, K.P. Ghoshal, Green synthesis of silver nanoparticles from *Butea-Monosperma* and their antimicrobial activities, *Bionano. Frontier* 5 (2) (2012) 7–11.
- [33] Y.C. Liu, L.H. Lin, New pathway for the synthesis of ultrafine silver nanoparticles from bulk silver substrates in aqueous solutions by sono electrochemical method, *Electrochem. Commun.* 6 (1) (2004) 1163–1168.
- [34] A.B. Smetana, K.J. Klabunde, C.M. Sorensen, Synthesis of spherical silver nanoparticles by digestive ripening, stabilization with various agents, and their 3-D and 2-D super-lattice formation, *J. Colloid Interface Sci.* 284 (1) (2005) 521–526.